Transient dynamics of nonlinear magneto-optical rotation in the presence of a transverse magnetic field

Raghwinder Singh Grewal[*] and Szymon Pustelny[†]
Institute of Physics, Jagiellonian University, Łojasiewicza 11, PL-30-348 Kraków, Poland

(Received 31 December 2019; accepted 24 February 2020; published 16 March 2020)

Nonlinear magneto-optical rotation is studied under nonequilibrium conditions. The polarization rotation of linearly polarized light, traversing a room-temperature rubidium vapor, is observed versus the time-dependent (swept) longitudinal magnetic field in the presence of static transverse magnetic fields. Presence of the transverse fields modifies the character of the observed signals. In particular, for the weaker fields, the longitudinal-field sweep leads to a two-frequency oscillation of the polarization rotation while crossing zero. Unlike the steady state, this was observed independent of the transverse-field direction. For the stronger transverse fields, the oscillations deteriorate eventually reaching a situation when a nonoscillating dynamic signal, with a distinct minimum close to the zero longitudinal field, is observed. The presented experimental results are supported with theoretical analysis based on the density-matrix formalism. The analysis confirms all the features of experimental results while providing an intuitive explanation of the observed behavior based on angular-momentum probability surfaces used for density-matrix visualization.

DOI: 10.1103/PhysRevA.101.033825

I. INTRODUCTION

Coherent interaction of resonant light with atoms results in an onset of many interesting optical phenomena including electromagnetically induced transparency [1], electromagnetically induced absorption [2,3], coherent population trapping [4,5], and nonlinear magnetic-optical rotation (NMOR) [6]. These effects are usually studied when an atomic system is in a steady state, where dynamic equilibrium between various processes is achieved. A specific example of such studies is NMOR [6–12], a process of rotation of linear polarization of light traversing an optically polarized medium subjected to a magnetic field [6]. At a microscopic level, NMOR can be explained as (i) initial optical pumping of atoms into an aligned state (generation of optical anisotropy in atoms) and (ii) successive evolution of the state due to magnetic field (precession of the anisotropy) or other parameters (e.g., rate of collisions), leading to further modifications of the state (e.g., anisotropy deterioration). Assuming that such parameters as magnetic field, light intensity, temperature, etc., are constant over time, a dynamic equilibrium between the processes is reached and static optical anisotropy of the medium is generated. In contrast to the steady-state case, NMOR under nonequilibrium conditions, i.e., when experimental parameters change faster than the characteristic time scale of a system, is studied less frequently [13–15]. Under such conditions, the contribution from various processes to the overall anisotropy of the medium leads to complex time-dependent dynamics resulting the signals that are significantly different from those observed in the conventional NMOR experiments.

Recently, theoretical and experimental studies of NMOR with time-dependent magnetic fields were performed [14]. In the studies, the polarization rotation of continuous-wave (CW) light, a illuminating rubidium vapor, was studied versus light intensity as well as magnitude and sweep rate of longitudinal magnetic field. The studies demonstrated that at low sweep rates, a traditional dispersive NMOR resonance, with a slight asymmetry between two sides of the signal, is observed. It was also shown that for faster sweep rates, the damped oscillations of the polarization-rotation signal are recorded. It was found that this behavior strongly depends on the magnetic-field sweep rate and that the same behavior is observed for different amplitudes and frequencies of the magnetic-field scans, corresponds, however, to the same sweep rate.

The aim of the present work is to study NMOR as a function of the time-dependent longitudinal magnetic field $B_z(t)$. In contrast to the previous work [14], however, the measurements are performed in the presence of the static magnetic field B_x or B_y, oriented transversely to the light-propagation direction. Presence of the transverse field modifies evolution of the system, resulting in changes of the observed NMOR signals. In particular, an additional modulation is observed when a weak transverse field is applied. It is also demonstrated that for the stronger transverse fields, the signals change their character. Under such conditions, not only the oscillations are suppressed, but also the shape of the signal envelop changes, becoming absorptive rather than dispersive. This behavior is observed experimentally and is confirmed with numerical simulations based on the density-matrix formalism. Visualization of the density matrix, using angular-momentum probability surfaces (AMPS), provides intuitive understanding of the observed dynamics, yet keeping all rigorousness of the quantum-mechanical treatment.

[*]raghugrewal.singh@gmail.com
[†]pustelny@uj.edu.pl

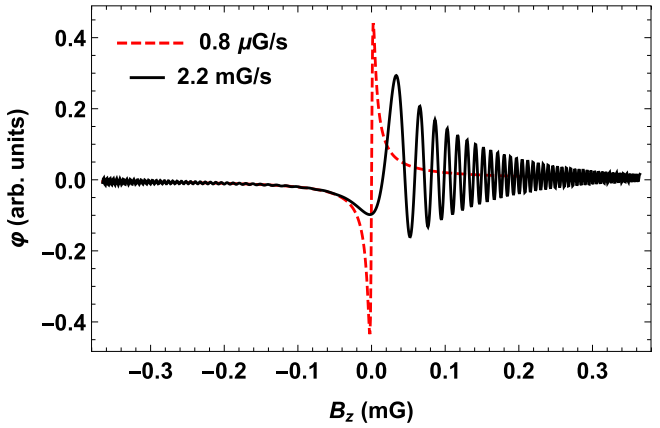

FIG. 1. Numerically simulated NMOR signals as a function of the longitudinal magnetic field $B_z(t)$ at different sweep rates (0.8 μG/s and 2.2 mG/s). The signals were simulated without the transverse fields ($B_x = B_y = 0$). The other parameters used in simulations are as follows: the optical Rabi frequency $\Omega_R/2\pi = 0.01$ MHz, the ground-state relaxation $\gamma/2\pi = 2.5$ Hz, and the excited-state relaxation of $\Gamma/2\pi = 5.75$ MHz. The oscillations seen on the left-hand side of the plot are an artifact of our simulation, which are performed for a continuously swept field with a triangular function. This type of the field scan was implemented to reproduce experimental conditions.

II. THEORETICAL RESULTS AND DISCUSSION

In our analysis, the NMOR signals are calculated using the density-matrix formalism. While details of the calculations can be found elsewhere (see, Ref. [14]), here we just recall their key elements. The analysis is performed in a $F = 2 \rightarrow F' = 1$ atomic system. The atoms interact with y-polarized light, propagating along the quantization axis z, with the wave vector k_z and of the amplitude E_y. The light-atom interaction is considered within the dipole approximation, in which interaction of light results in repopulation of ground-state magnetic sublevels and generation of Zeeman coherences between them. The time-dependent magnetic field $B_z(t)$, applied along the quantization axis, leads to energy splitting of the Zeeman sublevels. Here, we only consider the linear Zeeman effect due to a small value of the applied field. Simultaneously, the static fields B_x and B_y, generated in the transverse directions x and y, respectively, couples the magnetic sublevels. In the analysis, two types of relaxation are assumed. The first originates from spontaneous emission (density-matrix dependent relaxation) and the second is uniform relaxation, repopulating atoms toward the thermal equilibrium (density-matrix-independent relaxation). The time-dependent evolution of the density matrix is calculated within the rotating-wave approximation by numerically solving the Liouville equation. Next, the density matrix is used to calculate an angle of polarization rotation [16]. The refractive indexes $n_\pm$ for two orthogonal circular polarizations $\sigma^\pm$ are calculated using the density matrix, enabling determination of polarization rotation of linearly polarized light. While this model does not fully reproduce the experimental system, for example, it does not account for the fact that atoms freely travel between bright (illuminated) and dark regions of the cell, or more complex energy structure

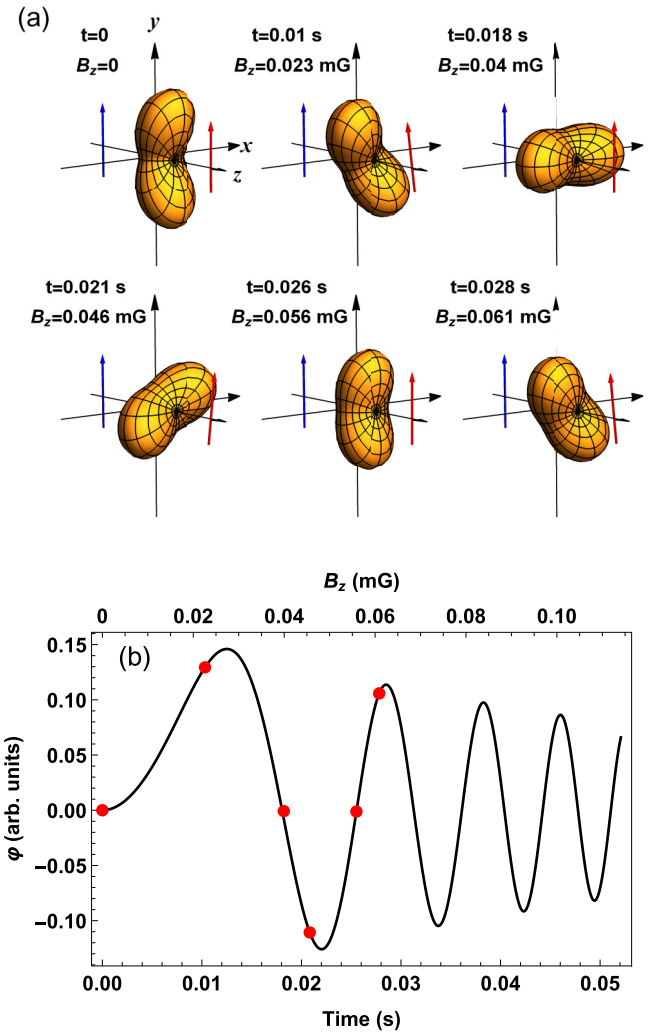

FIG. 2. (a) Angular-momentum probability surfaces illustrating temporal evolution of the density matrix. For clarity, at $t < 0$ interaction with strong pump light and no magnetic field was considered. This led to a strong atomic polarization shown for $t = 0$. Successive evolution of the system with the time-dependent magnetic field and much weaker probe light (pump light was switched off completely) was next considered ($t > 0$). The shapes present the successive stages of the evolution. (b) Corresponding signal of optical rotation as a function of time and instantaneous longitudinal magnetic field $B_z(t)$. Simulations are performed for the same set of parameters as in Fig. 1, including a sweep rate of 2.2 mG/s. Blue and red arrows in (a) show the polarization rotation angles before and after the medium. Red points marked on polarization-rotation curve in (b) are times t corresponding to the probability surface plots in (a).

(e.g., hyperfine levels), it still captures all essential features of the system.

Figure 1 presents numerically simulations of the NMOR signals at different magnetic-field sweep rates without any transverse fields. The plots show that at a low sweep rate, a dispersively shaped signal (red dashed curve), corresponding to a conventional (steady-state) NMOR experiment, is observed. When the sweep rate increases, the chirped damped oscillations are observed while crossing zero field (black solid curve). This behavior indicates that the medium evolves

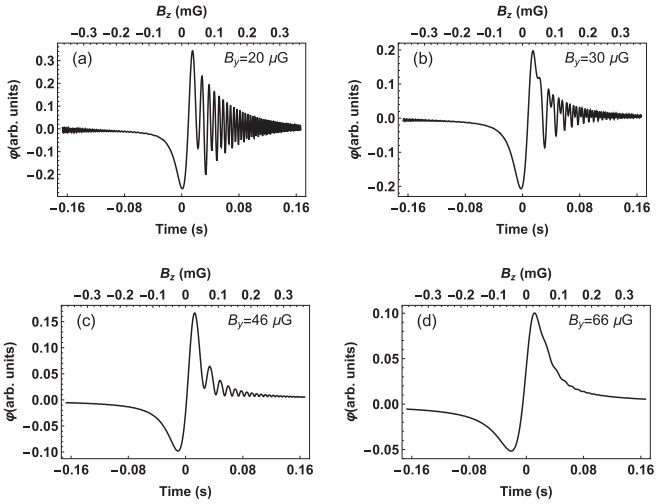

FIG. 3. NMOR signals simulated as a function of time and longitudinal magnetic field at a sweep rate of 2.2 mG/s and different B_y fields: (a) $B_y = 20$ μG, (b) $B_y = 30$ μG, (c) $B_y = 46$ μG, and (d) $B_y = 66$ μG. All calculations were performed for $B_x = 0$ and other parameters same as in Fig 1.

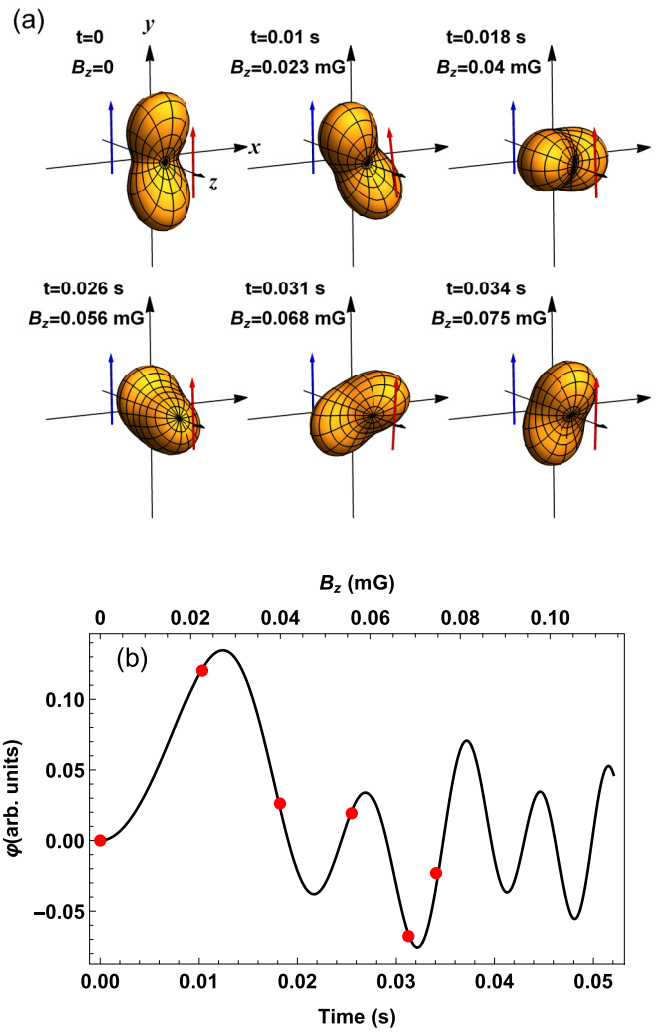

FIG. 4. (a) Angular-momentum probability surfaces illustrating evolution of the density matrix due to a combined action of the time-dependent longitudinal magnetic field $B_z(t)$ and static transverse magnetic field $B_y = 20$ μG ($B_x = 0$). (b) Corresponding optical rotation signal. Except B_y, the other parameters are the same as in Fig. 2.

toward a continuously changing equilibrium state without ever reaching the state. The chirping observed in the signal originates from temporal variation of the magnetic field, while the damping is a result of washing out medium optical anisotropy through combined action of magnetic field and light (see Ref. [14] for more details).

To investigate the quantum-mechanical evolution of the system, we present the density matrix at various stages of its evolution, using AMPS [17]. The surfaces provide a clear and intuitive understanding of some features of the system, capturing, for example, their spatial symmetries. In particular, the density matrix shown in Fig. 2(a), corresponding to the aligned state, is characterized with twofold rotational symmetry, i.e., the structure rotated by π around z reproduces itself. Hence, the optical signals observed at these two situations are the same. In turn, modulation of parameters of light observed with the magnetic field B_z leads to modulation of absorption and polarization rotation at twice the Larmor frequency.

Let us now consider the situation presented in Fig. 2(a). For clarity we assume that at $t < 0$ atoms interact with intense, linearly polarized pump light in absence of the magnetic field($\vec{B} = 0$). This leads to generation of strong optical anisotropy of the medium (atomic alignment) manifesting as a peanutlike density matrix [18]. At time $t = 0$, scanning of the longitudinal magnetic field B_z is turned on ($B_x = B_y = 0$) and the time evolution of the state is investigated in the presence of a weak probe beam. Figure 2(a) presents the probability surfaces corresponding to such evolution. The AMPS are plotted at different times [marked in Fig. 2(b) as red points] demonstrating various stages of the evolution.

The Zeeman interaction of atoms results in precession of their magnetic moments, which corresponds to the Larmor precession of the AMPS plots around the magnetic field(with the Larmor frequency $\Omega_L = \gamma B_z$, where γ is the gyromagnetic ratio of the atom). Since the magnetic field $B_z(t)$ rising over time, the precession frequency Ω_L also increases. Moreover, due to the relaxation and continuous (weak) optical pumping of the atoms, the system relaxes into a different state (with no Zeeman coherences), and anisotropy of the whole medium deteriorates (smaller contribution of a peanutlike part to the overall density matrix). In turn, the light experiences a weaker optical anisotropy of the medium, its polarization rotation gets smaller. Thereby, one observes slowly damped chirped oscillations of polarization rotation, which is presented in Fig. 2(b).

The situation changes when an additional transverse field is applied to the atoms. First, we considered the case when the transverse magnetic field B_y is applied along the light-polarization direction. In the case, the net magnetic field $\boldsymbol{B_{net}} = \boldsymbol{B_y} + \boldsymbol{B_z}(t)$ is oriented in the yz plane, i.e., the plane spanned by the light propagation direction and the axis of the peanut-like density matrix.

Figure 3 presents the rotation signals as a function of the time at different B_y. As shown, for the relatively weak transverse field ($B_y = 20\ \mu$G), a two-frequency [$\Omega_L(t)$ and $2\Omega_L(t)$] oscillation is observed. In the case, the $2\Omega_L$ oscillations dominate in the signal. Similar two-frequency oscillations were described in Ref. [19] and its time-independent (demodulated) counterpart was investigated in Ref. [20], under the steady state, where two-frequency oscillations manifested as resonances at Ω_L and $2\Omega_L$.

As B_y increases [Fig. 3(b)], the amplitude of the $2\Omega_L$ oscillation becomes smaller than the amplitude of the Ω_L oscillation. For stronger fields, $B_y \gtrsim 40\ \mu$G, the $2\Omega_L$ oscillation vanishes completely [Fig. 3(c)] and for even stronger fields ($B_y \gtrsim 60\ \mu$G) no oscillations (neither at Ω_L nor $2\Omega_L$) are observed in the NMOR signal [Fig. 3(d)]. This dependence on the transverse-field magnitude corresponds well to the steady-state situation, where an amplitude ratio of the Ω_L and $2\Omega_L$ resonances depend on the orientation of the magnetic field in the xy plane [20]. The origin of the two-frequency oscillations is explained by angular-momentum probability surfaces of the density matrix [Fig. 4].

Figure 4(a) shows the temporal evolution of the density matrix in the presence of B_y, while scanning the longitudinal field $B_z(t)$. At $t = 0$, the longitudinal magnetic field is zero, so the net field is oriented along the light polarization and atomic-alignment direction. Orientation of the magnetic field along the alignment axis does not modify the state of the atoms (the peanutlike shape is fully symmetric along the axis), and hence no polarization rotation is initially observed. As the longitudinal field $B_z(t)$ increases, the net magnetic field starts changing its direction, tilting in the yz plane toward z. Since it is no longer perpendicular to the alignment axis, the alignment starts to precesses around the instantaneous field. After a half of the Larmor period, the projection of this alignment onto the xy plane is parallel to the initial orientation [even though the two shapes are not aligned in three-dimensional (3D) space], however, its length (amplitude of the transverse-alignment projection onto the xy plane) is different from the initial case. As projection of the alignment on the xy plane determines the strength of optical anisotropy of the medium experience by the z-propagating light, the anisotropy of the medium is weaker. In turn, the induced polarization rotation is smaller. When the B_y field is not too strong, the initial state is better reproduced after another half of the Larmor period, i.e., the full precession period. Due to this, one observes two-frequency modulation of the rotation signal at $\Omega_L(t)$ and $2\Omega_L(t)$ [Fig. 4(b)]. On the top of the magnetic evolution, the processes of relaxation and repumping [21], leading to deterioration of the transverse alignment and damping of the oscillations is observed [Fig. 4(b)].

Next, the polarization rotation is calculated for different B_x but $B_y = 0$ (Fig. 5). As demonstrated in Ref. [20], under the steady state, such a constant field orientation leads to significantly different results as no resonance at Ω_L was observed. However, when the longitudinal field B_z is scanned, the behavior is different, i.e., two-frequency modulation is again observed [Fig. 5(a)]. In fact, for the weak transverse magnetic fields, the signals in the presence of B_y [Fig. 3(a)] and B_x [Fig. 5(a)] are similar (comparable amplitude ratio of the two frequency components). The only distinct feature

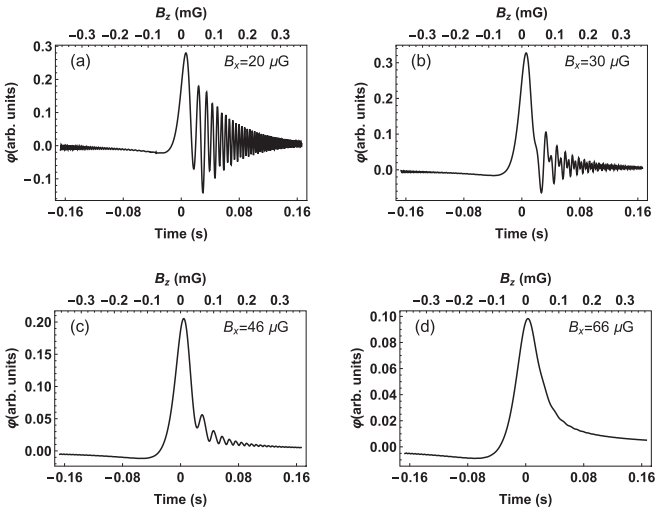

FIG. 5. Simulated NMOR signals as a function of the time and longitudinal magnetic field with a sweep rate of 2.2 mG/s at different values of the transverse field B_x: (a) $B_x = 20\ \mu$G, (b) $B_x = 30\ \mu$G, (c) $B_x = 46\ \mu$G, and (d) $B_x = 66\ \mu$G and $B_y = 0$. The other simulation parameters are identical as in the previous cases.

arises for negative magnetic field, i.e., in the case of $B_y > 0\ \mu$G and $B_x = 0$, the rotation is negative at $B_z(t) \lesssim 0\ \mu$G, but for $B_x > 0$ and $B_y = 0$, this negative rotation is strongly suppressed. The similarity between the two cases becomes less apparent for the stronger transverse fields. This is well visible in Figs. 5(b) and 5(c), where strong differences between envelopes of two signals but also amplitudes of two components [Fig. 5(b)] are observed. Finally, for the strongest fields ($B_x \gtrsim 60\ \mu$G), no oscillations are present in the rotation signal [Fig. 5(d)].

Figure 6(a) shows the time evolution of the density matrix in the presence of nonzero B_x and $B_y = 0$. At time $t = 0$, the longitudinal magnetic field is zero, so the net magnetic field is directed along the x axis. Since magnetic field is perpendicular to the alignment, it tilts the alignment in the yz plane, so that angle between alignment and light propagation direction is smaller than 90°. Although this tilt still does not produce any polarization rotation at time $t = 0$ [Fig. 6(b)], the situation resembles the case of $B_y \neq 0$ (it changes the projection of the alignment onto the xy plane). When the longitudinal field increases, the alignment tilted from the xy plane starts to precess around the instantaneous magnetic field, more precisely reproducing itself after full Larmor period than after half of the period. This process results in two-frequency components of the time-dependent rotation [Fig. 6(b)].

For completeness, Fig. 7 presents the polarization rotation signals when the magnetic fields B_x and B_y are simultaneously nonzero. The signals are calculated at different values of B_x with fixed B_y ($B_y = 20\ \mu$G). When B_x is less than B_y [Fig. 7(a)], the transient oscillations are similar to that observed in the signals shown in Fig. 3(a). As B_x increases, the signal becomes weaker [Fig. 7(b)], but, the amplitude of the positive rotation angles decreases more than of the negative angles. As B_x is further increased, the transient oscillations with negative rotation angles are only seen [Fig. 7(c)]. At the strongest B_x ($B_x \gg B_y$) [Fig. 7(d)], the oscillations

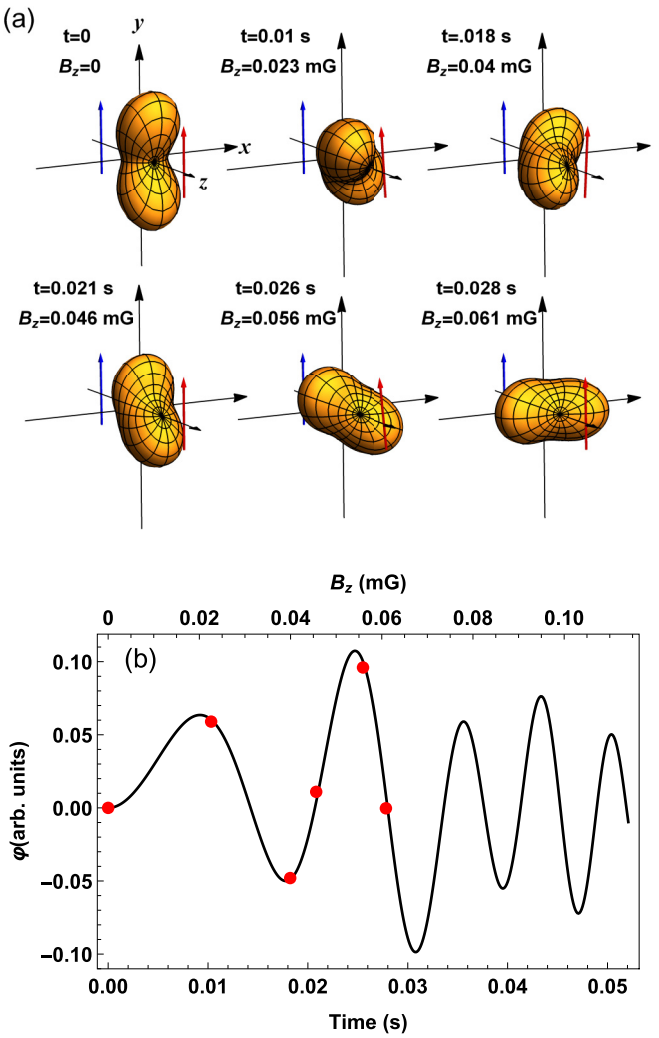

FIG. 6. (a) Angular-momentum probability surfaces illustrating the time-dependent dynamics of the density matrix and (b) corresponding optical rotation signal. The simulations are performed with $B_x = 20\ \mu$G and $B_y = 0$, and other simulation parameters unchanged with respect to the earlier simulations.

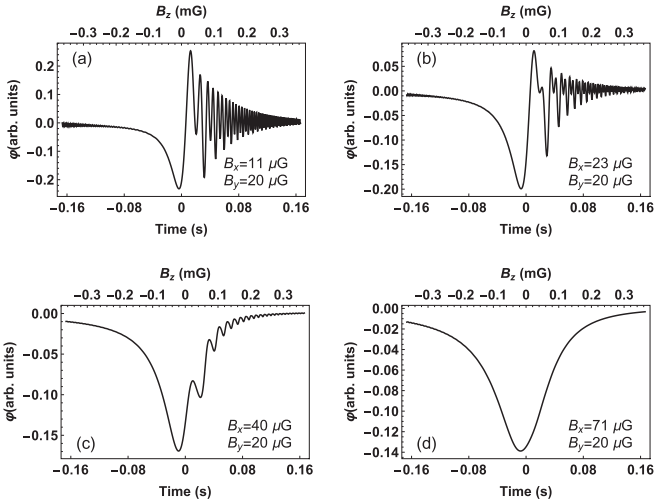

FIG. 7. Simulated NMOR signals versus time and magnetic field at a sweep rate of 2.2 mG/s, $B_y = 20\ \mu$G, and (a) $B_x = 11\ \mu$G, (b) $B_x = 23\ \mu$G, (c) $B_x = 40\ \mu$G, and (d) $B_x = 71\ \mu$G. Other parameters are identical as in previous simulations.

in the rotation signal vanishes and the shape of the signal changes to absorptive [Fig. 7(d)], which is different from the signals in Figs. 3(d) and 5(d).

In case of a two-level atom, the polarization rotation angle in the presence of a time-dependent longitudinal magnetic field and a static transverse magnetic field can be described as

$$\begin{aligned}\varphi = {} & \varphi_0 + \varphi_s e^{-\gamma_s (t-t_0)} + \varphi_{\Omega_L} e^{-\gamma_{\Omega_L}(t-t_0)} \\ & \times \sin\left[2\pi\left(\sqrt{\Omega_x^2 + S^2(t-t_0)^2}\right)(t-t_0) + \phi_1\right] \\ & + \varphi_{2\Omega_L} e^{-\gamma_{2\Omega_L}(t-t_0)} \\ & \times \sin\left[4\pi\left(\sqrt{\Omega_x^2 + S^2(t-t_0)^2}\right)(t-t_0) + \phi_2\right], \quad (1)\end{aligned}$$

where φ_0 corresponds to the time-independent rotation in the signal. The terms φ_s, φ_{Ω_L}, and $\varphi_{2\Omega_L}$ are the amplitudes of the static and oscillating at, Ω_L and $2\Omega_L$ contributions of the signals, respectively, and γ_s, γ_{Ω_L}, and $\gamma_{2\Omega_L}$ are the corresponding decay rates. The constants ϕ_1 and ϕ_2 are the initial phases of Ω_L and $2\Omega_L$ oscillations, respectively. Ω_x is the Larmor frequency of the transverse field B_x. S is the sweep rate of longitudinal magnetic field, given in G/s units. The constant t_0 is the zero-crossing time. Equation (1) has two components, static and oscillatory, which is discussed in detail in Ref. [14]. In addition to these to components, we have also considered the term φ_0, which accounts for the time-independent rotation in the signal at given sweep rate and transverse magnetic field. To study the Ω_L and $2\Omega_L$ dependences on the magnetic-field sweep rate in the presence of transverse field B_x, we first simulate the rotation signals at different sweep rates by keeping $B_x = 26\ \mu$G. The signals were fitted using Eq. (1) for time $t > t_0$, and the amplitudes φ_{Ω_L} and $\varphi_{2\Omega_L}$ are plotted as the function of the sweep rate [Fig. 8(a)]. As shown in Fig. 8(a), the increase in the sweep rate improves the $2\Omega_L$ oscillations and deteriorates the other component. A question one can ask in this context is if these amplitudes and their ratio depends on the other experimental parameters, e.g., laser intensity. This is analyzed in Fig. 8(b) which shows the ratio of φ_{Ω_L} and $\varphi_{2\Omega_L}$ at two different Rabi frequencies with fixed B_x. While a change of the Rabi frequency from 3 kHz to 10 kHz increases the amplitudes of both Ω_L and $2\Omega_L$ frequency components, the amplitude ratio of the components remains the same.

Figure 8(c) shows the amplitudes of both Ω_L and $2\Omega_L$ components for different transverse fields. When the transverse field is low, the Ω_L component rises with increasing magnetic field B_x. Somewhat surprisingly the amplitude of the $2\Omega_L$ component also increases with B_x and eventually reaching the maximum at $B_x = 8.6\ \mu$G. It was verified with additional simulations that the transverse field at which the maximum is reached depends on the sweep rate; the faster the rate the higher the transverse field at which it is reached. We believe that this initial increase comes from some competition between pumping of coherences and their destruction by the same beam (repumping). For zero

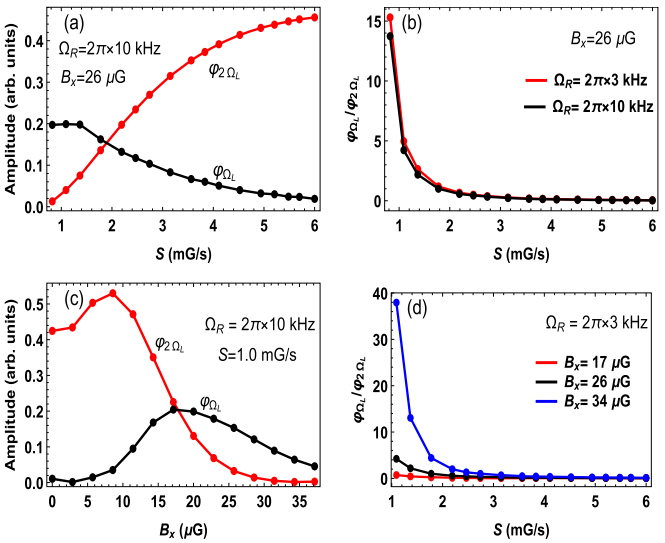

FIG. 8. (a) Amplitudes $\varphi_{2\Omega_L}$ and φ_{Ω_L} and (b) their ratio $\varphi_{\Omega_L}/\varphi_{2\Omega_L}$ as a function of the sweep rate at different Rabi frequencies with fixed B_x. (c) Amplitudes $\varphi_{2\Omega_L}$ and φ_{Ω_L} as the function of the transverse magnetic field B_x at fixed sweep rate S and Rabi frequency Ω_R. (d) The ratio $\varphi_{\Omega_L}/\varphi_{2\Omega_L}$ as a function of the sweep rate at different B_x for fixed Ω_R.

transverse fields the repumping process is efficient and hence smaller NMOR signals are observed. However, the complex evolution of atomic polarization at weak transverse fields reduces the efficiency of the repumping, effectively leading to increase of the NMOR-signal amplitude. Similar dependence, initial increase of the amplitude, maximum, and final deterioration is observed for the Ω_L component. Here, however, the process is more straightforward as at $B_x = B_y = 0$ there is no modulation at Ω_L, so any increase of transverse field from zero leads to increase of the Ω_L component. For larger transverse fields the pumping becomes less efficient, which results deterioration of the Ω_L component.

An important question is if one can use the ratio $\varphi_{\Omega_L}/\varphi_{2\Omega_L}$ to compensate or even determine the transverse magnetic field. To further investigate this issue we plot the amplitude ratio versus the sweep rate for the different transverse fields [Fig. 8(d)]. The presented plots demonstrate that the smaller the transverse field, less steep is the dependence. In particular, for $B_x = 0$ there will be only the $2\Omega_L$ component. This opens means for magnetometry of the transverse fields, which will be investigated independently elsewhere.

III. EXPERIMENTAL RESULTS AND DISCUSSION

Figure 9 shows the schematic diagram of the experimental setup. A diode laser (Toptica DL pro), emitting light of a wavelength of 795 nm with a linewidth of less than 1 MHz, is used. The light frequency is modulated at $\Omega_m/2\pi = 80$ kHz with a modulation depth of about 50 MHz to enable phase-sensitive detection and hence improve a signal-to-noise ratio of the observed signals. A half-wave plate $\lambda/2$ and a polarizing beam splitter PBS1, situated next to the laser, are used to

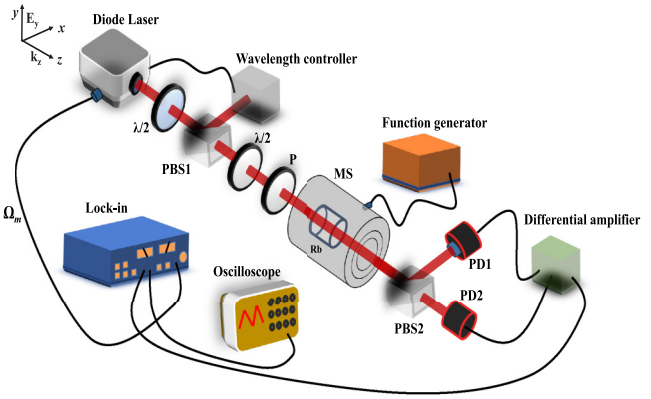

FIG. 9. Schematic diagram of the experiment. PBS1 and PBS2 are the polarizing beam splitters; $\lambda/2$ is the half-wave plate; P is the polarizer; MS is the magnetic shield; PD1 and PD2 are the photodetectors. The wavelength controller consists of the μDAVLL system and the wave meter.

control intensity of light directed into a dichroic atomic vapor laser lock (DAVLL), exploiting the micromachined vapor cell system [22], and a wave meter (HighFinesse/Angstrom Wavelength meter WS-U), used for wavelength stabilization and monitoring. The DAVLL setup is used to lock the light central frequency to the low-frequency wing of the Doppler-broadened $F = 2 \rightarrow F' = 1$ transition of the ^{87}Rb D_1 line. The intensity of light illuminating the rubidium vapor is set with the help of a half-wave plate $\lambda/2$ and a polarizer P. The main part of the light, polarized along the y direction, is sent through a paraffin-coated buffer-gas-free Rb vapor cell containing an isotopically enriched sample of ^{87}Rb. The vapor number density is around 10^9 atoms/cm^3 in the cell at the room temperature. The cell is placed at the center of a four-layer magnetic shield. The shield has three μ-metal layers and one innermost ferrite layer (Twinleaf MS-1LF). The magnetic shield compensates Earth's magnetic field by a factor of 10^6 at the location of the cell. To further reduce the magnetic field, the magnetic-field coils are installed inside the shield (not shown in Fig. 9). These coils are also used to scan the magnetic field along the light propagation direction (the z axis) with the help of a function generator. The coils are also used to apply transverse magnetic field along the x axis using a computer-controlled current source (DM Technology Multichannel Current Source). In our experimental setup, since the residual-field compensation coils are placed only along the x axis, a small residual field of the order of 14 μG is present inside the shield along the y axis ($B_r = B_y \approx 14$ μG).

The polarization rotation of light is measured using a balanced polarimeter setup, which contains a PBS2 and two photodiodes (PD1 and PD2). The PBS2 is rotated by 45° from the axis of the polarizer P and its outputs are measured using two photodiodes. The differential amplifier generates a difference signal which is demodulated with a lock-in amplifier at the first harmonic of the light modulation frequency. The time constant is small enough, not to affect the character of the observed dependencies. Finally, the lock-in output signal is recorded with an oscilloscope.

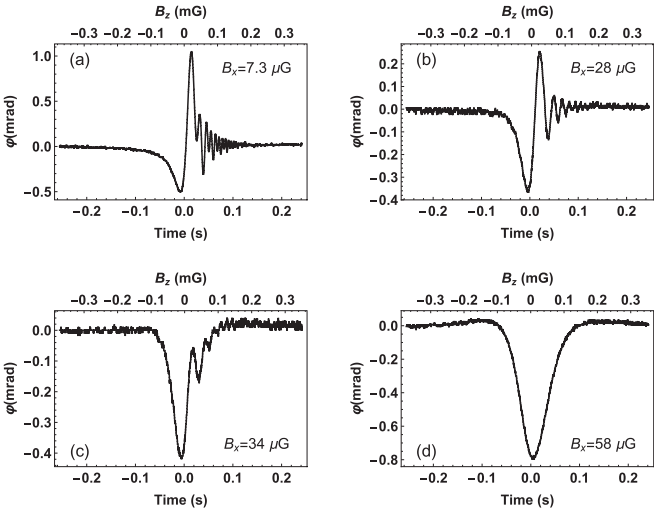

FIG. 10. Experimentally measured NMOR signals as a function of the time and longitudinal magnetic field swept at a rate of 1.5 mG/s. Measurements are performed at the constant transverse magnetic field $B_y \approx 14\ \mu$G and several different fields in x: (a) $B_x = 7.3\ \mu$G, (b) $B_x = 28\ \mu$G, (c) $B_x = 34\ \mu$G, and (d) $B_x = 58\ \mu$G. The signals are measured with a light intensity of 2 μW/mm^2 before the cell.

Figure 10 shows the experimentally observed transient behavior at different B_x in the presence of residual magnetic along the y axis. The longitudinal magnetic field $B_z(t)$ is varied at a sweep rate of 1.5 mG/s. The results reveal a good agreement with theoretical calculations (Fig. 7). Small transverse fields modify the transient rotation signals and create the two-frequency damped oscillations of polarization rotation [Fig. 10(a)].

With a constant field ($B_y \approx 14\ \mu$G) along the y axis, the oscillations at twice the Larmor frequency vanish and the amplitude of the positive rotation decreases when B_x is increased. Importantly, the strength of negative angles remains almost unchanged [Fig. 10(b)]. When B_x increased further, no rotation at positive angle is observed [Fig. 10(c)] and the shape of the signal becomes absorptive [Fig. 10(d)]. This is a behavior that was also shown in Fig. 7.

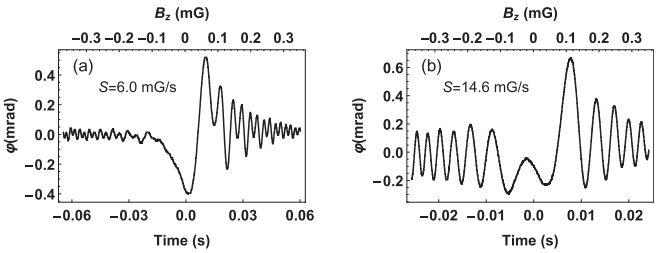

FIG. 11. Experimentally measured NMOR signals as functions of the time and longitudinal magnetic field swept at a rate of (a) 6.0 mG/s and (b) 14.6 mG/s. The other experimental parameters are the same as in Fig. 10(b). The oscillations observed at the left side of the resonance is the artifact of our measurement procedure (see Ref. [14] for more details).

The residual magnetic field B_y is very small, so it merely affects the signals at higher sweep rates in the absence of B_x. The effect of transverse fields at given values decreases when the sweep rate of signal is increased by keeping all other experimental parameters (light power, cell temperature, etc.) unchanged. For example, if the sweep rate in Fig. 10(b) is increased, the oscillations at twice of the Larmor frequency reappears [Fig. 11(a)]. As the sweep rate is further increased, the oscillations at the Larmor frequency disappear and the signal with a single-frequency oscillation [Fig. 11(b)], similar to that measured in the absence of the transverse fields, can be seen.

IV. CONCLUSION

The transient dynamics of nonlinear magneto-optical rotation in a paraffin-coated rubidium vapor cell was studied in the presence of constant magnetic fields perpendicular to the light-propagation direction. The two-frequency oscillations in the transient polarization-rotation signals were observed for both transverse fields B_x and B_y (parallel or perpendicular to the light polarization direction). As demonstrated, the behavior of the signals differs from the steady-state NMOR signals, where the two frequencies can be seen only when the transverse field is parallel to the light-polarization direction. We explained the observations by using the angular probability surface of the density matrix of atoms. According to the explanation, when the transverse field is applied perpendicular to the light-polarization direction, the atomic alignment tilts towards the light-propagation direction at an instantaneous longitudinal field close to zero. Hence, the angle between the atomic-alignment axis and the net magnetic field becomes less than 90° and the situation becomes similar to the case when the transverse field is parallel to light-polarization axis. We demonstrated that the atomic alignment returns to its original state in the full Larmor period for both transverse fields. The amplitude of the oscillations at twice the Larmor frequency starts decreasing with increase of any transverse field as the angle between net magnetic field and alignment orientation gets smaller. For stronger fields, the rotation signals without oscillations are observed. When both transverse fields are nonzero at the same time, the shape of the signals changes significantly. We observed the rotation signal with no transient oscillations and with minima near zero scanning field.

In this experiment, a small transverse field leads to the transient signals of different character than without the field. Therefore, by scanning the longitudinal field one may detect the transverse field *in situ*, and then compensate it by minimizing the Ω_L-frequency component in the signal. With this respect, the effect can be used for precise compensation of the magnetic field and hence offers a possibility to extract full vectorial information of the magnetic field in a single measurement. Compensation of the field also enables decrease of the transverse relaxation rate of atoms.

Long relaxation times are also important for quantum-information storage, specific quantum-information-processing protocols (e.g., those employing optical dipole

traps [23]) and even single-photon sources [24]. In this context, the ability to precisely compensate transverse magnetic fields using a simple single-beam experiment may be particularly attractive.

ACKNOWLEDGMENTS

The work was supported from the grants of the National Science Centre, Poland within the OPUS program (Project No. 2015/19/B/ST2/02129).

[1] M. Fleischhauer, A. Imamoglu, and J. P. Marangos, Rev. Mod. Phys. **77**, 633 (2005).
[2] A. Lezama, S. Barreiro, and A. M. Akulshin, Phys. Rev. A **59**, 4732 (1999).
[3] R. S. Grewal and M. Pattabiraman, J. Phys. B: At. Mol. Opt. Phys. **48**, 085501 (2015).
[4] K. Nasyrov, S. Cartaleva, N. Petrov, V. Biancalana, Y. Dancheva, E. Mariotti, and L. Moi, Phys. Rev. A **74**, 013811 (2006).
[5] R. S. Grewal and M. Pattabiraman, J. Phys. B: At. Mol. Opt. Phys. **47**, 195501 (2014).
[6] D. Budker, W. Gawlik, D. F. Kimball, S. M. Rochester, V. V. Yashchuk, and A. Weis, Rev. Mod. Phys. **74**, 1153 (2002).
[7] D. Budker, D. F. Kimball, S. M. Rochester, V. V. Yashchuk, and M. Zolotorev, Phys. Rev. A **62**, 043403 (2000).
[8] D. Budker, D. F. Kimball, V. V. Yashchuk, and M. Zolotorev, Phys. Rev. A **65**, 055403 (2002).
[9] Y. P. Malakyan, S. M. Rochester, D. Budker, D. F. Kimball, and V. V. Yashchuk, Phys. Rev. A **69**, 013817 (2004).
[10] I. Novikova, A. B. Matsko, and G. R. Welch, J. Opt. Soc. Am. B **22**, 44 (2005).
[11] T. Zigdon, A. D. Wilson-Gordon, S. Guttikonda, E. J. Bahr, O. Neitzke, S. M. Rochester, and D. Budker, Opt. Express **18**, 25494 (2010).
[12] S. Pustelny, L. Busaite, M. Auzinsh, A. Akulshin, N. Leefer, and D. Budker, Phys. Rev. A **92**, 053410 (2015).
[13] M. U. Momeen, G. Rangarajan, and V. Natarajan, Phys. Rev. A **81**, 013413 (2010).
[14] R. S. Grewal, S. Pustelny, A. Rybak, and M. Florkowski, Phys. Rev. A **97**, 043832 (2018).
[15] G. Jin, Y. Xu, and Z. Wang, Opt. Express **27**, 7087 (2019).
[16] M. Auzinsh, D. Budker, and S. M. Rochester, *Optically Polarized Atoms* (Oxford University Press, Oxford, 2010).
[17] S. M. Rochester and D. Budker, Am. Journ. Phys. **69**, 450 (2001).
[18] For time-dependent magnetic field at $t < 0$ the anisotropy would contain a significant spherical contribution, which would make it harder to capturing dynamics of the system.
[19] L. Lenci, A. Auyuanet, S. Barreiro, P. Valente, A. Lezama, and H. Failache, Phys. Rev. A **89**, 043836 (2014).
[20] S. Pustelny, W. Gawlik, S. M. Rochester, D. F. Jackson Kimball, V. V. Yashchuk, and D. Budker, Phys. Rev. A **74**, 063420 (2006).
[21] The anisotropy axis of atoms pumped with linearly polarized light is oriented along its polarization. At the same time, instantaneously after generation of the polarization, the polarization starts to evolve due to magnetic field (anisotropy precession around the magnetic field). Since individual-atom pumping occurs at distinct times, CW pumping and precession leads to smearing out orientations over different directions, which effectively leads to deterioration of net transverse anisotropy. The faster the precession, the more efficient the washing out of the medium's net anisotropy. Therefore, this leads to smaller rotation of light polarization and deterioration of the NMOR signal with increasing magnetic field.
[22] S. Pustelny, V. Schultze, T. Scholtes, and D. Budker, Rev. Sci. Instrum. **87**, 063107 (2016).
[23] C. Weitenberg, S. Kuhr, K. Mølmer, and J. F. Sherson, Phys. Rev. A **84**, 032322 (2011).
[24] M. Dąbrowski, M. Mazelanik, M. Parniak, A. Leszczyński, M. Lipka, and W. Wasilewski, Phys. Rev. A **98**, 042126 (2018).